ADVANCED MATERIALS

DOI: 10.1002/adma.200602326

A High-Performance Magnetic Resonance Imaging T_2 Contrast Agent**

By *Jian Qin*, *Sophie Laurent*, *Yun Suk Jo*, *Alain Roch*, *Maria Mikhaylova*, *Zaver M. Bhujwalla*, *Robert N. Muller*, and *Mamoun Muhammed**

Magnetic resonance imaging (MRI) has been recognized as one of the best noninvasive imaging modalities in both clinical and research fields because of its ability to provide a wealth of spatial and temporal information with excellent resolution.[1] The MRI mechanisms are based on excitation and relaxation of hydrogen nuclei that are abundant in water and lipids of tissue. Intrinsic longitudinal (T_1) and transverse (T_2) relaxation times of different parts of the tissues bring about changes of MR signal intensity, which in turn results in an imaging contrast. The relaxation times can be manipulated by the use of T_1 (e.g., gadolinium or manganese chelates) and T_2 (e.g., particulate iron oxide) contrast agents, producing brighter (T_1-weighted) and darker (T_2-weighted) images where they are accumulated.[2,3] Several types of superparamagnetic iron oxide nanoparticles (SPIONs) have been developed as MRI contrast-enhancing agents with biocompatible surface coatings.[4–8] Such particles are usually prepared through a conventional co-precipitation method in the aqueous phase,[9–12] however, some physical characteristics of the nanoparticles, such as broad size distribution and aggregation, still need to be improved. Recently, high-temperature decomposition strategies have been developed to produce monodisperse and highly crystalline iron oxide nanoparticles.[13–15] However, their uses are quite limited because the particles synthesized by these methods can only be dispersed in nonpolar organic solvents because of the long alkyl chain of the capping molecules. Thus, only a few examples of developing such particles as MRI contrast agents have been reported.[16,17] For biomedical applications, it is indispensable to transfer these nanoparticles to an aqueous phase. Several studies have dealt with a variety of methodological improvements including ligand exchange with tetramethylammonium hydroxide (TMAOH),[18] dimercaptosuccinic acid (DMSA),[19] phosphine oxide polymers, [20] and dendrons[21] to enhance stability of nanoparticles in aqueous solution. Alternatively, a layer of amphiphilic molecules such as poly(maleic anhydride-*alt*-1-tetradecene),[22] surfactant/lipid,[23] and α-cyclodextrin[24] have been used to form an intercalating structure with the hydrophobic capping molecules on the particle surface. In these cases, the second layer of amphiphilic molecules is coupled with the first layer of capping molecules through the hydrophobic interaction, whilst the other side of the amphiphilic molecule renders the particles to be dispersible in aqueous phase.

Inspired by the aforementioned intercalation scheme, we have developed a facile method to transfer the hydrophobic SPIONs to water by employing Pluronic F127 (PF127). PF127 is an ABA-type triblock copolymer consisting of poly(propylene oxide) (PPO) and poly(ethylene oxide) (PEO). The PF127 block copolymer is selected as a suitable candidate of surface modification because it is recognized as being highly biocompatible (approved by the Food and Drug Administration)[25,26] and has been used in experimental medicine and pharmaceutical sciences for a long period of time.[27–30] Labhasetwar and co-workers recently reported a novel magnetic drug-delivery system by incorporating PF127 and oleic acid with iron oxide nanoparticles prepared through the co-precipitation approach.[31,32] Unlike Labhasetwar's work, our as-synthesized SPIONs are intrinsically coated with a layer of oleic acid. Upon addition of PF127 copolymer, the PPO block in the middle of the PF127 molecule associates with the alkyl tail of the oleic acid through the hydrophobic interaction, while the two appending PEO chains solubilize the particles in aqueous media by virtue of their high hydrophilicity (Fig. 1a–c). The obtained water-soluble particles have a hierarchical surface structure (denoted as PF127/oleic acid@superparamagnetic iron oxide nanoparticles, hereafter abbreviated as POA@SPION).

[*] Prof. M. Muhammed, J. Qin
Materials Chemistry Division, Royal Institute of Technology
10044 Stockholm (Sweden)
E-mail: mamoun@mse.kth.se
Dr. S. Laurent, Dr. A. Roch, Prof. R. N. Muller
Department of General, Organic and Biomedical Chemistry
NMR and Molecular Imaging Laboratory
Universitè de Mons-Hainaut
7000 Mons (Belgium)
Y. S. Jo
Institute of Bioengineering (IBI)
École Polytechnique Fédérale de Lausanne (EPFL)
1015 Lausanne (Switzerland)
Dr. M. Mikhaylova, Prof. Z. M. Bhujwalla
JHU ICMIC Program
The Russell H. Morgan Department of Radiology and Radiological Science
The Johns Hopkins University School of Medicine
Baltimore, MD 21205 (USA)

[**] This work has been partially supported by the European Commission 6th Framework Program (InnoMed LSHB-CT-2005-518170) (Swedish group) and in part by the ARC Program (00/05-258) of the French Community and of the Region of Wallonia (NOMADE Project) (Belgian group). Supporting Information is available online from Wiley InterScience or from the authors.

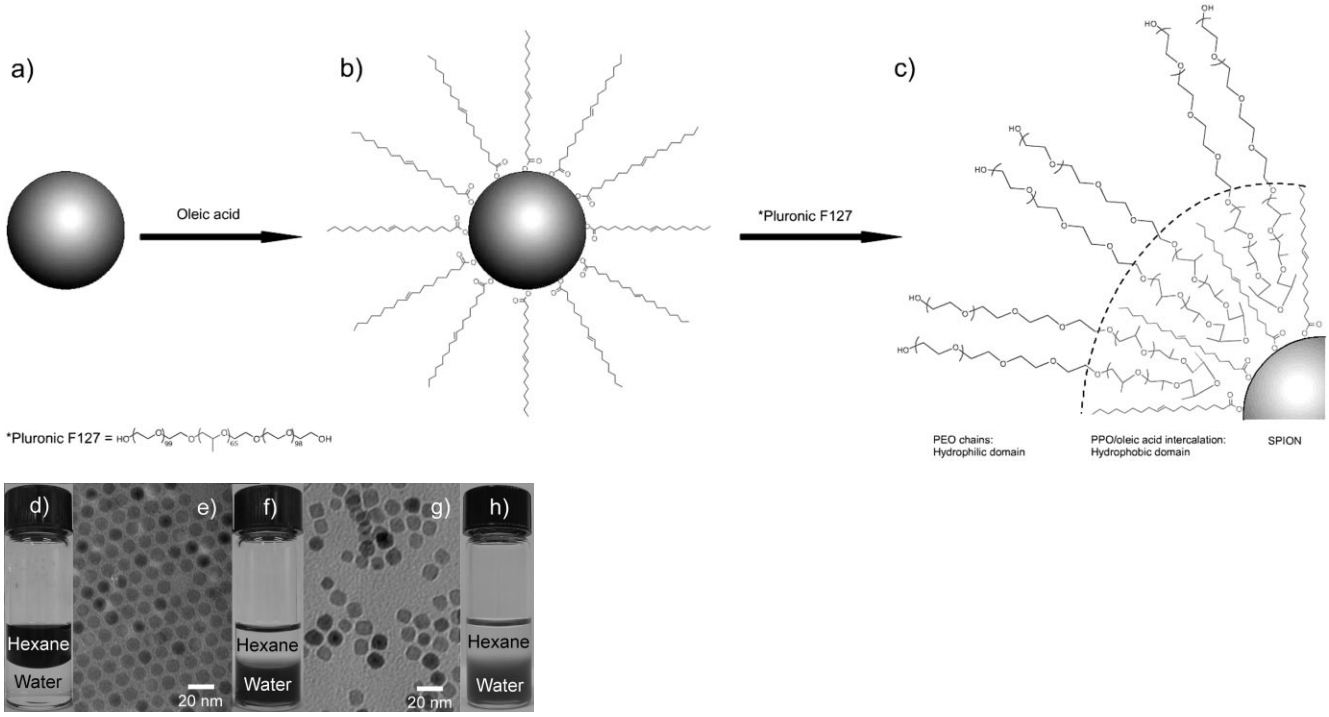

Figure 1. The evolution of the hierarchical structure: a) pristine SPION, b) as-synthesized SPION coated with oleic acid, c) SPION with hierarchical coating after phase transfer by PF127. Photographs of the particle distribution d) before and f) after phase transfer. TEM images of SPION in e) hexane and g) water. h) Photograph of POA@SPION in water shows a stable dispersion after four months.

Transmission electron microscopy (TEM) images show that the SPIONs are monodisperse both in hexane and water (Fig. 1e and g). Figure 1d and f demonstrates the complete phase transfer from the organic to the aqueous phase. There was no significant change in the size and shape of the particles as a result of the phase transfer. The homogeneous morphology was retained in a regular round shape with an average diameter of 10.1 nm ($\sigma \approx 4.5\,\%$). In long-term stability tests, no agglomeration was observed in a colloidal solution after several months, as shown in Figure 1h. The crystal structure of the SPIONs was identified by using X-ray diffraction (XRD; Fig. S1 in Supporting Information). The peaks are labeled with the indexed Bragg reflections of the maghemite structure and the particles are found to be highly crystalline. Using the Debye–Scherrer formula, the average size of the crystallite is determined to be 9.3 nm, which is in good agreement with the average diameter measured from TEM images, indicating that the particles are single crystalline. The magnetic properties of the iron oxide nanoparticles were examined at room temperature by using a vibrating sample magnetometer (VSM). The magnetization of both as-synthesized SPIONs and POA@SPION were measured as a function of an applied magnetic field (Fig. 2). From the magnetization measurements, little change in the magnetic properties was observed between the as-synthesized SPIONs and those after the phase transfer. None of the samples showed a hysteresis, indicating that the nanoparticles retain the superparamagnetic property. The saturated magnetization (*Ms*) of as-synthesized SPIONs

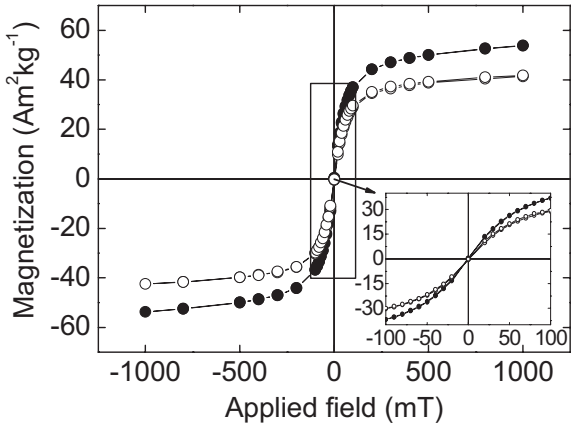

Figure 2. Room-temperature magnetization curve of as-synthesized SPIONs (●) and POA@SPION (○).

and POA@SPION are 53.12 and 41.58 A m^2 kg^{-1}, respectively. Fitting the data in Figure 2 to the Langevin equation,[33] we obtained diameters of the magnetic cores of as-synthesized SPIONs and POA@SPION equal to 9.98 and 11.1 nm, which is very close to the value obtained from both TEM and XRD data.

Fourier-transform infrared (FTIR) spectra of POA@SPION were recorded to confirm the presence of a hierarchical coating layer consisting of PF127 and oleic acid on the surface of the nanoparticles (Fig. S2). The FTIR spectrum of oleic acid

ADVANCED MATERIALS

shows strong characteristic peaks, assigned to the CH_2 chain at 2893 (asymmetric stretching, ν_a C–H), 2841 (symmetric stretching, ν_s C–H), and 1460 (scissoring, δ_s C–H) cm^{-1}. A peak corresponding to the C=O asymmetric stretch of the ester of oleic acid was observed at 1720 cm^{-1}. The peak at 1111 cm^{-1} can be interpreted as the characteristic C–O–C stretch of PF127. The characteristic peaks from both oleic acid and PF127 were clearly identified in the spectrum of POA@SPION, indicating the presence of both molecules on the particle surface. The formation of a double layer on the surface was further verified by thermogravimetric analysis (TGA) and differential scanning calorimetry (DSC) (Figs. S3 and S4). The TG curve of POA@SPION shows that two distinct steps of weight loss occur at 210 °C and 355 °C, corresponding to the evaporation temperature of oleic acid and the decomposition temperature of PF127, respectively. From the TG analysis, the weight percentage of the coating molecules was estimated: ca. 6 % for oleic acid and ca. 15 % for PF127. The DSC data for pure PF127 showed a strong endothermic peak, indicating the melting point as 56.2 °C. Comparatively, a small endothermic peak at 48.7 °C for POA@SPION resulted from melting of the PF127 coating layer on the nanoparticles. The lower melting point could be due to the intercalation structure formed between PF127 and oleic acid molecules. As a consequence, the degree of crystallinity of the PF127 polymer decreased, hence decreasing the melting point of the attached PF127 layer.

Since the MRI contrast agents are intended for systemic administration, it is of great significance to minimize the toxicity of the particles. Samples of POA@SPION with three different iron concentrations, ranging from 1 to 100 $\mu g\,mL^{-1}$, were incubated with the HeLa and MCF-12A cell lines for 48 h. The viability of the cells was evaluated by MTS (3-(4,5-dimethylthiazol-2-yl)-5-(3-carboxymethoxyphenyl)-2-(4-sulfophenyl)-2*H*-tetrazolium) and MTT (3-(4,5-dimethylthiazol-2-yl)-2,5-diphenyltetrazolium bromide) assays and the results showed no significant cytotoxicity to the mitochondria function for both cell types (Fig. 3).

To check the efficiency of POA@SPION as a novel T_2 contrast agent, the relaxation times T_1 and T_2 were measured at 0.47 T (20 MHz proton Larmor frequency, 37 °C) and 1.41 T (60 MHz proton Larmor frequency, 37 °C) respectively. The T_1 (spin–lattice) relaxation process results from the interaction between the excited nuclei and their surrounding environment and the T_2 (spin–spin) relaxation process results from the interaction between the excited nuclei and those with lower energy. The efficiency of an MRI contrast agent is commonly assessed in terms of its relaxivities r_1 and r_2, which are rates of proton relaxation and are determined according to the equation

$$1/T_{i,obs} = 1/T_{i,d} + r_i\,[M]\ (i = 1, 2) \quad (1)$$

where $1/T_{i,obs}$ is the observed solvent relaxation rate in the presence of a contrast agent, $1/T_{i,d}$ is the relaxation rate of the pure diamagnetic solvent, and [M] is the concentration of the contrast agent.[34] For a T_2 contrast agent, the higher the r_2/r_1 ratio, the better the contrast efficacy. The relaxivities of POA@SPION are summarized in Table 1 and are compared to those obtained under the same conditions using commercial T_2 contrast agent Resovist (Schering AG, Germany). Noticeably, the r_2/r_1 ratios of POA@SPION are 6- and 17-fold higher than those of Resovist at 0.47 T (20 MHz) and 1.41 T (60 MHz), respectively, indicating that POA@SPION is a T_2 contrast agent with high efficiency.

Noting that the magnetic cores of POA@SPION and Resovist are produced via different methods, we also investigated the relaxivities of SPION transferred to an aqueous phase by coating the particles with small molecule layers, for example, TMAOH[37] and DMSA.[19] From Table 1, it is clear that the relaxivities and r_2/r_1 ratios of TMAOH@SPION and DMSA@SPION are similar to those of Resovist. Hence, the enhancement of the r_2/r_1 ratios is believed to result from the surface characteristics of POA@SPION. The r_1 of POA@SPION is 20 and 30 times lower than those of Resovist and Feridex (Advanced Magnetics, Cambridge, Massachusetts), respectively, while the r_2 of POA@SPION is of the same order of magnitude with the commercial contrast agents. As a result, the r_2/r_1 ratio of POA@SPION is much higher than the commercial contrast agents.

Based on the relaxometry results, it is hypothesized that the PF127/OA hierarchical structure plays a dual role to simultaneously maintain the T_2 relaxation rate and to decrease the T_1 relaxation rate. As shown in Figure 1c, the voluminous hydrophilic PEO domain facilitates the diffusion of large amount of water molecules in the vicinity of the magnetic core of POA@SPION, which consequently results in the large T_2 relaxation rate.[38] Furthermore, it has been reported that the T_2 relaxation rate of ice is very high.[39] Similarly, in the hierarchical structure, the mobility of water molecules in the diffusing layer is restricted because of hydrogen bonding between the water molecules and the hydrophilic chains of the PEO blocks, resulting in large amount of "icelike" water. Therefore, the large r_2 relaxivity of POA@SPION is a result of "icelike" water in the hydrophilic blocks. The dimension of the "diffusing layer" of POA@SPION can be characterized as the

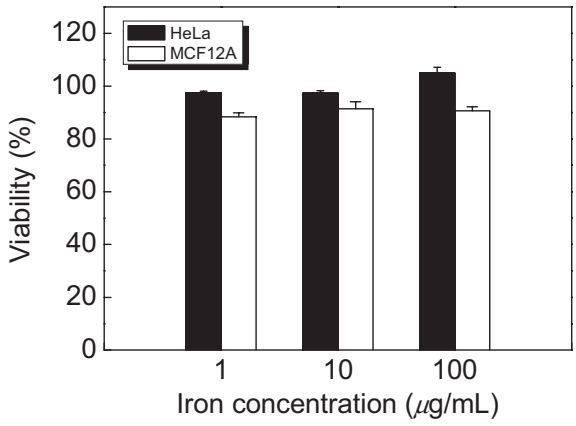

Figure 3. Cell viability of HeLa and MCF-12A cells after 48 h incubation with POA@SPION at various iron concentrations.

Table 1. Surface coatings, mean hydrodynamic diameters, and relaxivities of SPIONs with different coatings, Resovist measured at 20 MHz (0.47 T) and 60 MHz (1.41 T) in water (37 °C), and reported relaxivity values for Resovist and Feridex.

Sample name	Surface coating	Mean hydrodynamic diameter [nm]	20 MHz			60 MHz		
			r_1 [$s^{-1}mM^{-1}$]	r_2 [s^{-1} mM^{-1}]	r_2/r_1	r_1 [s^{-1} mM^{-1}]	r_2 [s^{-1} mM^{-1}]	r_2/r_1
POA@SPION	PF127/OA	71	1.33	63.4	47.7	0.311	71.3	229
TMAOH@SPION	TMAOH	–	22.3	156	7.00	9.70	175	18.0
DMSA@SPION	DMSA	–	8.01	67.8	8.46	2.6	76.7	29.5
Resovist [a]	Carboxydextran	65	24.9	177	7.10	10.9	190	17.4
Resovist [35]	Carboxydextran	65	25	164	6.2	–	–	–
Feridex [36]	Dextran	72	40	160	4	–	–	–

[a] From this work.

mean hydrodynamic diameter, which is similar to the other contrast agents (Table 1). It has been reported that the r_2 values can be greatly increased by clustering T_2 contrast agents in reservoirs such as liposomes or cells.[40] This effect results from the intrinsic mechanism of spin–spin relaxation, which relies on the local concentration of the contrast agents. However, POA@SPION shows no enhancement to the local Fe concentration because it forms a well-dispersed and stable colloid as evidenced by TEM studies. Moreover, the small r_2 value compared to those exceedingly high ones for clustered particles in micelles provides additional evidence that POA@SPION are not agglomerated.[40] Conversely, T_1 contrast agents require immediate contact with the water molecules to effectively expedite T_1 relaxation due to the inherent mechanism of spin–lattice relaxation.[41] As seen in Figure 1c, the magnetic core of POA@SPION is segregated from the exterior water molecules by a compact hydrophobic layer comprised of PPO blocks and oleic acid molecules. Water molecules diffused into the PEO domain can hardly come into contact with the magnetic core because of the hydrophobic nature of the inner layer. Such a hierarchical hydrophobic–hydrophilic coating of POA@SPION is substantially different from the conventional T_2 contrast agents whose coating layers are entirely hydrophilic so that the diffusion of water molecules to magnetic core is not restricted. The covalent bond between the carboxylic group of oleic acid and iron oxide ensures complete coverage of the particle surface. The subsequent incorporation of PF127 molecules further increases the thickness of this hydrophobic "isolating layer". Such a structure comprised of PPO blocks and oleic acid molecules would effectively hinder the external water molecules from contact with the magnetic core, which in turn kinetically limit the spin–lattice relaxation rate.

In conclusion, monodisperse SPIONs were transferred from an organic phase to an aqueous solution through modification of the oleic acid coated SPION surface with PF127 copolymers. This methodology allows no significant alteration of the morphology, monodispersity, crystallinity, and magnetic properties of the as-synthesized nanoparticles. In comparison with commercial magnetic nanoparticles, POA@SPION showed a high r_2/r_1 ratio. Based on our findings, it is suggested that the PF127/oleic acid hierarchical coating layer plays a critical role in enhancing the r_2/r_1 ratio. Therefore, a particulate iron oxide with exceptional monodispersity and high crystallinity would greatly extend their applications to the biomedical realm.

Experimental

Sample Preparation: Details are described in Supporting Information. Briefly, SPIONs were synthesized by the decomposition of iron oleate complex ($Fe(oleate)_3$) in a high-boiling-point solvent (dioctyl ether, $T_B = 287$ °C), with small modifications of methods reported in the literature [42]. In order to prepare PF127-coated water-soluble iron oxide nanoparticles, a concentrated suspension of as-synthesized SPIONs dispersed in hexane was mixed with an aqueous solution containing an appropriate amount of PF127 followed by vigorous agitation for 30 min. The obtained solution was dried under argon gas flow overnight, resulting in a fine powder of POA@SPION, which is readily dispersible in water. The aqueous solution of nanoparticles was then dialyzed against 1 L of deionized water for 48 h to remove unbound PF127 polymers.

MR Relaxometry Measurements: Relaxivity r_1 (20 and 60 MHz) was measured at 0.47 T with a Minispec PC-20 Brucker spectrometer and 1.41 T with Mq Series systems; r_2 was measured with Minispec (20 and 60 MHz) on spectrometer AMX-300.

Cell Viability Tests: Typically, POA@SPION was lyophilized for 72 h. Three different concentrations of the solutions were sequentially prepared by diluting the stock solution with the appropriate amount of cell media. HeLa and MCF-12A cells were prepared at a density of 5×10^4 cells per mL of medium in case of HeLa cells and 5×10^3 cells per mL of medium for MCF-12A. The prepared cells were seeded 200 μL in each well of a 96-well microplate. The cells were incubated with various concentrations of particles for 48 h. Cells without any nanoparticles were seeded and cultivated in the same way and used as controls. The medium was removed and replaced with 100 μL of growth medium prior to the addition of the 20 μL/well of CellTiter 96 AQueous One Solution Reagent (Promega) based on an MTS assay for HeLa cells. After the plate was incubated for 4 h at 37 °C, the plates were read using a microplate reader (Tecan Safire2) at 570 nm with a reference wavelength of 630 nm. In case of MCF-12A, 10 μL of an MTT dye solution was added to each well and cells were incubated for three more hours. Afterwards, 100 μL of detergent reagent was added and plates were kept in the dark overnight. The absorbance was read on a microplate reader (Dynatech MR7000 instruments) at 550 nm.

Received: October 13, 2006

[1] J. C. Richardson, R. W. Bowtell, K. Mäder, C. D. Melia, *Adv. Drug Delivery Rev.* **2005**, *57*, 1191.
[2] Y. Okuhata, *Adv. Drug Delivery Rev.* **1999**, *37*, 121.

[3] A. C. Silva, J. H. Lee, I. Aoki, A. P. Koretsky, *NMR Biomed.* **2004**, *17*, 532.
[4] A. Bjørnerud, L. Johansson, *NMR Biomed.* **2004**, *17*, 465.
[5] P. Reimer, B. Tombach, *Eur. J. Radiol.* **1998**, *8*, 1198.
[6] R. Weissleder, G. Elizondo, J. Wittenberg, C. A. Rabito, H. H. Bengele, L. Josephson, *Radiology* **1990**, *175*, 489.
[7] D. D. Stark, R. Weissleder, G. Elizondo, P. F. Hahn, S. Saini, L. E. Todd, J. Wittenberg, J. T. Ferrucci, *Radiology* **1988**, *168*, 297.
[8] D. K. Kim, M. Mikhaylova, F. H. Wang, J. Kehr, B. Bjelke, Y. Zhang, T. Tsakalakos, M. Muhammed, *Chem. Mater.* **2003**, *15*, 4343.
[9] R. Massart, *IEEE Trans. Magn.* **1981**, *17*, 1247.
[10] R. A. Whitehead, M. S. Chagnon, E. V. Groman, L. Josephson, *US. Patent 4 554 088*, **1985**.
[11] D.-B. Shieh, F.-Y. Cheng, C.-H. Su, C.-S. Yeh, M.-T. Wu, Y.-N. Wu, C.-Y. Tsai, C.-L. Wu, D.-H. Chen, C.-H. Chou, *Biomaterials* **2005**, *26*, 7183.
[12] Y. Sahoo, A. Goodarzi, M. T. Swihart, T. Y. Ohulchanskyy, N. Kaur, E. P. Furlani, P. N. Prasad, *J. Phys. Chem. B* **2005**, *109*, 3879.
[13] J. Rockenberger, E. C. Scher, A. P. Alivisatos, *J. Am. Chem. Soc.* **1999**, *121*, 11 595.
[14] T. Hyeon, S. S. Lee, J. Park, Y. Chung, H. B. Na, *J. Am. Chem. Soc.* **2001**, *123*, 12 798.
[15] N. R. Jana, Y. Chen, X. Peng, *Chem. Mater.* **2004**, *16*, 3931.
[16] H.-T. Song, J.-S. Choi, Y.-M. Huh, S. Kim, Y.-W. Jun, J.-S. Suh, J. Cheon, *J. Am. Chem. Soc.* **2005**, *127*, 9992.
[17] Y.-M. Huh, Y.-W. Jun, H.-T. Song, S. Kim, J.-S. Choi, J. H. Lee, S. Yoon, K.-S. Kim, J.-S. Shin, J.-S. Suh, J. Cheon, *J. Am. Chem. Soc.* **2005**, *127*, 12 387.
[18] L. E. Euliss, S. G. Grancharov, S. O'Brien, T. J. Deming, G. D. Stucky, C. B. Murray, G. A. Held, *Nano Lett.* **2003**, *3*, 1489.
[19] Y.-W. Jun, Y.-M. Huh, J.-S. Choi, J.-H. Lee, H.-T. Song, S. Kim, S. Yoon, K.-S. Kim, J.-S. Shin, J.-S. Suh, J. Cheon, *J. Am. Chem. Soc.* **2005**, *127*, 5732.
[20] S.-W. Kim, S. Kim, J. B. Tracy, A. Jasanoff, M. G. Bawendi, *J. Am. Chem. Soc.* **2005**, *127*, 4556.
[21] M. Kim, Y. Chen, Y. Liu, X. Peng, *Adv. Mater.* **2005**, *17*, 1429.
[22] T. Pellegrino, L. Manna, S. Kudera, T. Liedl, D. Koktysh, A. L. Rogach, S. Keller, J. Rädler, G. Natile, W. J. Parak, *Nano Lett.* **2004**, *4*, 703.
[23] H. Fan, E. W. Leve, C. Scullin, J. Gabaldon, D. Tallant, S. Bunge, T. Boyle, M. C. Wilson, C. J. Brinker, *Nano Lett.* **2005**, *5*, 645.
[24] Y. Wang, J. F. Wong, X. Teng, X. Z. Lin, H. Yang, *Nano Lett.* **2003**, *3*, 1555.
[25] J. Liaw, Y.-C. Lin, *J. Controlled Release* **2000**, *68*, 273.
[26] S. M. Shishido, A. B. Seabra, W. Loh, M. G. de Oliveira, *Biomaterials* **2003**, *24*, 3543.
[27] R. M. Nalbandian, R. L. Henry, K. W. Balko, D. V. Adams, *J. Biomed. Mater. Res.* **1987**, *21*, 1135.
[28] T. P. Johnston, S. C. Miller, *J. Parenter. Sci. Technol.* **1985**, *39*, 83.
[29] A. V. Kabanov, E. V. Batrakova, D. W. Miller, *Adv. Drug Delivery Rev.* **2003**, *55*, 151.
[30] A. V. Kabanov, E. V. Batrakova, N. S. Melik-Nubarov, N. A. Fedoseev, T. Y. Dorodnich, V. Y. Alakhov, V. P. Chekhonin, I. R. Nazarova, V. A. Kabanov, *J. Controlled Release* **1992**, *22*, 141.
[31] T. K. Jain, M. A. Morales, S. K. Sahoo, D. L. Leslie-Pelecky, V. Labhasetwar, *Mol. Pharm.* **2005**, *2*, 194.
[32] M. A. Morales, T. K. Jain, V. Labhasetwar, D. L. Leslie-Pelecky, *J. Appl. Phys.* **2005**, *97*, 10Q905.
[33] C. P. Bean, J. D. Livingston, *J. Appl. Phys.* **1959**, *30*, 120S.
[34] N. Bloembergen, E. M. Purcell, R. V. Pound, *Phys. Rev.* **1948**, *73*, 679.
[35] T. Allkemper, C. Bremer, L. Matuszewski, W. Ebert, P. Reimer, *Radiology* **2002**, *223*, 432.
[36] L. Josephson, J. Lewis, P. Jacobs, P. F. Hahn, D. D. Stark, *Magn. Reson. Imaging* **1988**, *6*, 647.
[37] V. Salgueiriño-Maceira, L. M. Liz-Marzán, M. Farle, *Langmuir* **2004**, *20*, 6946.
[38] P. A. Hardy, R. M. Henkelman, *Magn. Reson. Imaging* **1989**, *7*, 265.
[39] J. G. Georgiadis, M. Ramaswamy, *Int. J. Heat Mass Transfer* **2005**, *48*, 1064.
[40] H. Ai, C. Flask, B. Weinberg, X. Shuai, M. D. Pagel, D. Farrell, J. Duerk, J. Gao, *Adv. Mater.* **2005**, *17*, 1949.
[41] S. L. Fossheim, A. K. Fahlvik, J. Klaveness, R. N. Muller, *Magn. Reson. Imaging* **1999**, *17*, 83.
[42] J. Park, K. An, Y. Hwang, J.-G. Park, H.-J. Noh, J.-Y. Kim, J.-H. Park, N.-M. Hwang, T. Hyeon, *Nat. Mater.* **2004**, *3*, 891.